Multi-Time Co-optimization of Voltage Regulators and Photovoltaics in Unbalanced Distribution Systems

Ibrahim Alsaleh [iD] , *Student Member, IEEE,* Lingling Fan [iD] , *Senior Member, IEEE*

Abstract—In distribution systems with high penetrations of solar energy, co-optimizing the operation of voltage regulators (VRs) with off-unity power factor inverters of photovoltaics (PVs) becomes imperative for confining nodal voltages within ANSI limits and ensuring an adequate number of tap actions. The framework proposed in this paper minimizes the energy import from the substation (or maximizes the solar utility), the line losses, and the diurnal VR actions (VRAs) to reduce their maintenance costs and optimally coordinate with PV Var compensation. This is subject to the physical and security constraints of unbalanced distribution systems for which we build upon the rank-relaxed semidefinite programming branch flow model (SDP BFM). Departing from approximate VR models, we formulate an accurate model with nonuniformly-operated discrete tap positions. We overcome the computational complexity of solving the multi-time MISDP problem and the trilinearity emanating from VR incorporation by the application of Generalized Benders Decomposition (GBD). Also, to efficiently accommodate a large instance of binary variables, we accelerate the GBD's convergence with additional constraints on tap positions to reduce the search region. The merits of the proposed algorithm are demonstrated on the modified IEEE 37-bus and 123-bus test feeders for an hourly day-ahead optimization.

Index Terms—voltage regulators, multi-time co-optimization, generalized benders decomposition, semidefinite programming.

NOMENCLATURE

A. Sets and Indices

$i \in \mathcal{B}$	Set of buses.
$i \in \mathcal{B}^+$	Set of descent buses from the substation, where $\mathcal{B}^{\mathrm{s/g}}$ denote sets of VR secondary-side/PV buses.
$(i,j) \in \mathcal{L}$	Set of distribution lines.
Φ_i	Set of existing phases at bus i, $\Phi_i \subseteq \{a,b,c\}$.
ϕ	Indices of vector variable entries.
$\phi\phi$	Indices of matrix variable diagonal entries.
$t \in \mathcal{T}$	Set of scheduling time.

B. Parameters

z_{ij}	Line impedance linking bus i to bus j [p.u.].
s_i^{d}	Real/Reactive power demand at bus i [p.u.].
$r^{\min}/r^{\max}$	Minimum/maximum ratio limit.

I. Alsaleh is is with the Department of Electrical Engineering, University of Hail, Hail 55476, Saudi Arabia, and also with the Department of Electrical Engineering, University of South Florida, Tampa, FL 33620, USA (e-mail: ialsaleh@usf.edu).

L. Fan is with the Department of Electrical Engineering, University of South Florida, Tampa, FL 33620, USA (e-mail: linglingfan@usf.edu).

Δ^r	Ratio change per tap.
M	Large number.
V_{nom}	Nominal voltage at the substation bus.
$\underline{V}/\overline{V}$	Minimum/maximum voltage magnitude [p.u.].
s^{max}	PV inverter's apparent-power capacity [p.u.].
p^{for}	Solar power forecast at $i \in \mathcal{B}^{\mathrm{g}}$ [p.u.].
c_{pri}	Cost of minimizing power import and losses.
c_{vr}	Cost of minimizing voltage regulator actions.
$\mathbf{v}_i$	Vector of primary-side voltage quantities from accumulated iterations.

C. Variables

V_i/v_i	Voltage vector/Hermitian matrix at bus i [p.u.].
I_{ij}/ℓ_{ij}	Current vector/Hermitian matrix of line (i,j) [p.u.].
S_{ij}	Power flow matrix of line (i,j) [p.u.].
$r_{i'}/\hat{r}_{i'}$	Tap ratio vector/symmetric matrix variables.
s_i^{g}	PV complex power at $i \in \mathcal{B}^{\mathrm{g}}$ [p.u.].
$u_{i'}$	Binary variables used to to represent tap positions.
$\xi_{i'}$	Auxiliary variable used to to linearize bilinear terms.
$\lambda_{i'}$	Dual variable of the VR voltage equality constraint of SP.
$\mu_{i'}$	Dual variable of the VR voltage equality constraint of FCP.
$w_{i'}$	Symmetric auxiliary matrix variable to relax the VR voltage constraint of FCP.
η	Continuous variable of the lower bound objective.
F_{ij}	Power flow PSD marix of line (i,j).
G_i	PSD marix of PV inverter's capacity limit at bus $i \in \mathcal{B}^{\mathrm{g}}$.
x	Continuous variables of the SP and FCP.
y	Mixed-integer variables of the MP.

LIST OF ABBREVIATIONS

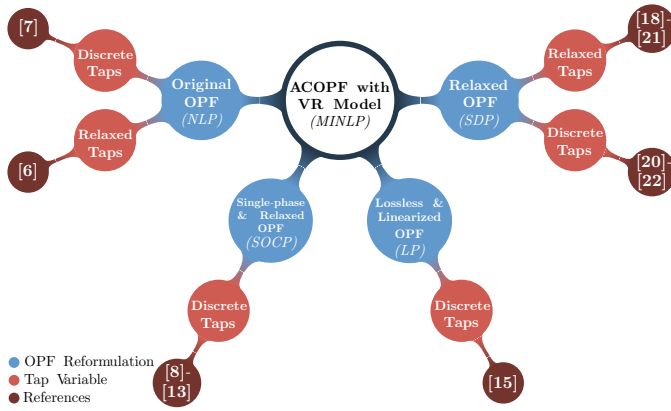|	
VR	Voltage regulator
PV	Photovoltaic.
VRA	Voltage regulator action
BFM	Branch flow model
SDP	Semidefinite programming
SOCP	Second order conic programming
MILP	Mixed-integer linear programming
GBD	Generalized Benders decomposition
SP	Subproblem
MP	Master problem

Fig. 1: Model-based scheduling problems and VR model considerations in the literature. None of the SDP-based papers consider inter-temporal VRAs.

I. INTRODUCTION

THE distribution system continues to undergo a proliferation of distributed generators, e.g., solar PVs. While PVs are instrumental in reducing the energy demand and losses, rising and fluctuating voltage issues have been largely attributable to their immoderate and intermittent real power injections. In response, voltage regulators (VRs) are challenged to re-adjust more frequently to adapt to the net demand. The excessive cycling wears and tears the apparatus, subsequently increasing the maintenance costs and shortening their life span. On the other hand, power-electronic inverters interfacing renewables have recently been sanctioned by technical standards to partake in the voltage support due to their fast-acting reactive power supply/absorption (less than 10 ms). Reference [1] contends that simultaneous scheduling of discrete and continuous devices is vital to account for their interaction with one another over a long planning horizon. Hence, advanced computational tools are demanded to capitalize on the inverters to coordinate with VRs and reduce their actions for security and economic purposes. With the deployment of smart meters and dispatchable inverters, the distribution system operator (DSO) can attain a coordinated operation along with circuit-wide objectives by centrally performing an offline model-based optimization problem leveraging alternating current optimal power flow (ACOPF) models with a forecast of loading and supply. The offline model-based scheduling problem in [2] has shown potential for using sufficiently-capacitated PV inverters to limit daily VRAs, consequently reducing the maintenance costs by more than half. Other dispatch methods rely on rule-based [3], zone-based [4], and measurement-based [5] techniques.

The nonconvex equality constraints of the multiphase power flow equations along with discrete mechanical settings of voltage regulation equipment results in a mixed-integer non-linear programming (MINLP) problem, which is NP-hard. Considering the inter-temporal VRAs adds to the complexity of the problem. In what follows, the current state-of-the-art on VR incorporation is surveyed. Fig. 1 provides the categorization of the reference papers.

Current State-of-the-art Reference [6] explores to solve the problem with relaxed integer variables and a rounding scheme to minimize the substation energy. In [7], the energy loss is minimized considering a high PV penetration in an MINLP problem solved with the application of predictor-corrector primal-dual interior point method (PCPDIPM). However, global optimal solutions are theoretically not guaranteed with NLP problems. To bypass the computational difficulties and initializations of NLP formulations, various simplifications with regard to the ACOPF have been exploited to lend a convex OPF model and a more computationally-affordable problem. For example, accurate discrete models on single-phase distribution feeders are prevalent in the literature [8]–[13], thanks to the advent of the second-order conic programming relaxation for the branch flow model (SOCP BFM) that promises global optimality for exact solutions [14], and the maturity of MISOCP solvers. The fact that feeders are composed of inherently-unbalanced loads and untransposed lines is yet of major significance and substantive to the mathematical replication to provide useful insights into the dispatch. In [15], the discrete assets are optimally set based on a lossless multiphase ACOPF, where a linear approximation is carried out to obtain an MILP problem. This approximation can however compromise the viability of the solution.

In contrast, the works in [16], [17] constitute two notable convexifications of multiphase ACOPF models based on the rank relaxation of a semidefinite program. Only recently have ideal VRs (with continuous and discrete taps) been incorporated by [18]–[22] into these convex models, focusing on *single-time* scheduling only.

In [18]–[21], the tap positions are assumed to take continuous values. This is realized in [18] merely by confining the diagonal of the secondary-side voltage within the tap ratio range. However, the arbitrariness of secondary-side phase angles that stems from this relaxation may cause solutions to deflect from rank-1. Recently, reference [19] employs the McCormick envelopes to linearize the ratio-voltage constraint with explicit continuous tap ratio variables. The relaxation is tightened with prior assumptions on phase angles and valid equality constraints. The experiments however reveal that the relaxed problem cannot guarantee rank-1 solutions. References [20], [21] propose linear SDP constraints that overcome the phase-angle issue, though impose uniformly-operated taps. The tap ratios are implicitly formed by the SDP constraints, making it difficult to control their cycling.

Although challenging, encoding the accurate VR model into the multi-phase convex ACOPF models is essential to exhibit the tap-changing process. Besides, rounding heuristics for continuous tap positions can lead to sub-optimal and infeasible solutions, as discussed in [6], [8] and demonstrated in [10, Section II-A2]. References [20], [21] also investigated discrete tap position modeling with uniform tap positions over the three phases. Compared to the nonuniformly-operated taps, exposition [23] shows that uniform tap operation does not conform to the system's unbalances and yields lower loss reductions. Exact incorporation of nonuniform discrete tap operation into the SDP BFM has been first modeled in [22]. Nonetheless, the need to solve optimization-based bound tightening (OBBT) problems prior to the GBD and the excessive number of binary variables are an additional computational burden and unsuited for the multi-time scheduling problem.

Therefore, more efficient incorporation of discrete VR models into the SDP BFM is required. Further, the multi-time co-optimization of VRs and PVs, where PV Vars are urged to minimize VRAs, has not yet been studied on the convex multi-phase OPF models.

Contributions: Motivated by the former limitations, this paper proposes a customized GBD-based algorithm that provides a global optimal multi-time scheduling of VRs and PVs over an hourly horizon window, accurately internalizes the discrete nature of three-phase VR model with independently-controlled tap positions (33 tap ratio per phase), and reduces the inter-temporal VRAs, which can ultimately be achieved via re-adjustments of continuous PV Var compensation throughout the scheduling horizon.

Details of our contributions can be summarized as follows.

1) A multi-time co-optimization of VRs and PVs is formulated which integrates detailed discrete tap positions into the state-of-the-art SDP-BFM model to minimize VRAs. The binary expansion technique, presented in [8] for single-phase tap changers, is extended to the multiphase BFM. Because of the VRA reduction objective, the problem is spanned across the entire scheduling horizon. To the best of our knowledge, accounting for the multi-time coordinated operation with VRA reduction on the SDP-based multiphase ACOPF have not been accomplished by the literature.

2) An efficient solving algorithm based on GBD is designed. The subproblem (SP) is decoupled by the prediction time intervals and computed sequentially, and the multi-cut master problem (MP) solves the tap ratio variables and inter-temporal VRA reduction objective. The problem separation not only provides an alternative to integrate the binary variables, but also sidesteps the non-convexities and the rank conundrum originating from the VR incorporation.

3) Enhancement of GBD convergence is designed for the specific structure of the problem. The convergence is improved by adding constraints to the master problem that bind the tap ratios by the voltage limits.

Organization: The ensuing sections are organized as follows. Section II describes the OPF equations and presents the voltage regulation models and PV Var capability. Section III describes the application of the GBD to solve the MISDP-based problem. Section IV provides the case studies on the modified IEEE 37-bus and 123-bus feeders to corroborate the merits of the proposed method to globally minimize the operating cost with coordinated scheduling of VRs and PVs.

II. PROBLEM FORMULATION

In this section, we review the multiphase BFM, introduce the VR and PV models, and set the objectives for the proposed multi-time scheduling problem. For brevity, the time index, t, is removed from modeling subsections.

A. Branch Flow Model

Consider a radial distribution system (each bus has a distinct parent) represented by the graph $\mathcal{G}(\mathcal{B}, \mathcal{L})$. The root bus, whose

voltage is set to V_{nom}, is denoted as 0, thus $\mathcal{B}^+ = \mathcal{B} - \{0\}$. In what follows, we use the Ohm's law to derive the matrix-based SDP BFM constraints [16].

1) Ohm's Law: The voltage drop on (i, j) is

$$V_j = V_i - z_{ij}I_{ij} \tag{1}$$

where V_i, V_j, and $I_{ij} \in \mathbb{C}^{|\Phi_j|}$, while $z_{ij} \in \mathbb{C}^{|\Phi_j| \times |\Phi_j|}$. When both sides are multiplied by their Hermitian transposes, and $v_i = V_iV_i^{\text{H}}$, $v_j = V_jV_j^{\text{H}}$, $S_{ij} = V_iI_{ij}^{\text{H}}$ and $\ell_i = I_{ij}I_{ij}^{\text{H}}$ are defined, (1) can be re-expressed as

$$v_j = v_i - (S_{ij}z_{ij}^{\text{H}} + z_{ij}S_{ij}^{\text{H}}) + z_{ij}\ell_{ij}z_{ij}^{\text{H}}, \quad \forall \ (i, j) \in \mathcal{L}. \tag{2}$$

In this form, actual phase angles are implicit in the nondiagonal complex entries of the surrogate variables, whereas diagonal entries represent the squared voltage magnitudes (real values).

2) Power Balance: For each $i \to j \to k$, to interpret the power balance at j, (1) is multiplied by I_{ij}^{H}:

$$V_jI_{ij}^{\text{H}} = V_iI_{ij}^{\text{H}} - z_{ij}I_{ij}I_{ij}^{\text{H}}, \tag{3}$$

$$V_j\Big(\sum_{(j,k)\in\mathcal{L}} I_{jk}^{\text{H}} + I_j^{\text{H}}\Big) = S_{ij} - z_{ij}\ell_{ij}, \tag{4}$$

where I_j is the net current at bus j. The net load power at bus j is $s_j \in \mathbb{C}^{|\Phi_j|}$, and thus the power balance is expressed as the diagonal of (4):

$$\sum_{(j,k)\in\mathcal{L}} \text{diag}(S_{jk}) + s_j = \text{diag}(S_{ij} - z_{ij}\ell_{ij}), \quad \forall(i, j) \in \mathcal{L}. \tag{5}$$

3) PSD and Rank-1 Matrix: The following positive and rank-1 $2|\Phi| \times 2|\Phi|$ matrix, written in a 2×2 block, are essential for the power flow constraint ($v_i \odot \ell_{ij} = S_{ij} \odot S_{ij}^{\text{H}}$, where $\odot$ is an element-wise multiplication operator).

$$F_{ij} = \begin{bmatrix} v_i & S_{ij} \\ S_{ij}^{\text{H}} & \ell_{ij} \end{bmatrix} \succeq 0 \qquad \forall \ (i, j) \in \mathcal{L} \tag{6}$$

$$\text{rank}(F_{ij}) = 1 \qquad \forall \ (i, j) \in \mathcal{L} \tag{7}$$

where $\succeq$ enforces the positive semidefiniteness (all matrix eigenvalues are nonnegative).

4) Convexification: The rank-1 constraint (7) is removed from the set of constraints to arrive at a convex problem. The solution of each F_{ij} should however promise a close proximity to rank1, for which an exactness check will be conducted on the results in Section IV-C2.

B. Voltage Regulator Model

A three-phase VR consists of three single-phase autotransformers, each equipped with an independent tap changer to regulate the system unbalances. The primary circuit is connected to bus i, and a virtual bus is introduced to the system, $i' \in \mathcal{B}^{\text{s}}$, to represent the secondary side. Fig. 2a shows a per-phase autotransformer on $(i, j) \in \mathcal{L}$. The tap ratios $r_{i'} \in \mathbb{R}^{|\Phi_j|}$ are modeled as decision variables so as to adjust the secondary-side and descent voltage levels. Given that the VR impedance is too small [24], an ideal VR is assumed.
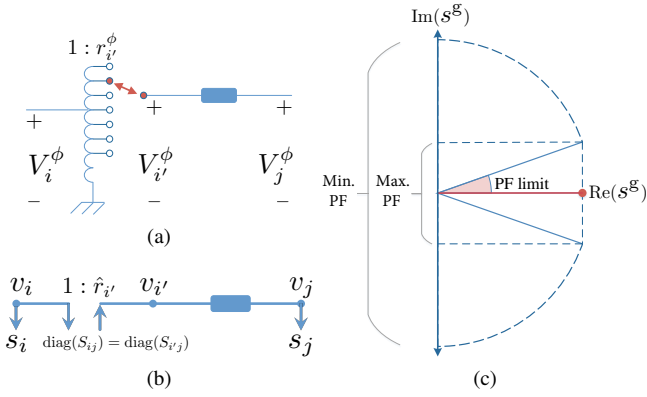
Fig. 2: (a) Per-phase tap-changing model. (b) Variable representation in SDP-based BFM. (c) Var capability of a variable-PF PV inverter.

1) Per-phase VR model: Let $|\mathcal{K}|$ be the number of positions the tap can take, i.e. typically ± 16 and a neutral position, $\mathcal{K} = \{k|k = 0, 1, 2, \ldots, 32\}$. Then, the per-phase discrete adjustment process is reflected by the following:

$$r_{i'}^{\phi} = \sum_{k=0}^{\mathcal{K}} (r^{\min} + \Delta^r \times k) u_{i',k}^{\phi} \qquad \forall i' \in \mathcal{B}^s \quad (8a)$$

$$\sum_{k=0}^{\mathcal{K}} u_{i',k}^{\phi} = 1 \qquad \forall i' \in \mathcal{B}^s \quad (8b)$$

where $\Delta^r = (r^{\max} - r^{\min})/|\mathcal{K}|$. To enforce the ratio selection, a vector of 33 binary variables, $u_{i'}$, is multiplied by all possible each ratio, and the sum to 1 results in a single ratio. The formulation in (8) requires 99 of binary variables for each three-phase VR. For fewer variables, the binary expansion technique [8] is adopted, and (8) is reformulated as:

$$r_{i'}^{\phi} = r^{\min} + \Delta^r \sum_{e=0}^{\mathcal{E}} 2^e u_{i',e}^{\phi} \qquad \forall \ i' \in \mathcal{B}^+ \quad (9)$$

where $\mathcal{E} = \{e|e = 0, 1, \ldots, 5\}$. In this form, only $|\mathcal{E}| = 6$ binary variables are needed to construct 33 possible tap ratios, and a total of 18 binary variables for each three-phase VR.

2) Secondary-side voltage constraint: To integrate the tap ratio model into the SDP BFM, the secondary-side voltage constraint is expressed as:

$$v_{i'} = (r_{i'} r_{i'}^{\mathsf{T}}) \odot v_i = \hat{r}_{i'} \odot v_i \qquad \forall \ i' \in \mathcal{B}^s \quad (10)$$

It is easily observed that the newly-defined ratio variable, $\hat{r}_{i'} \in \mathbb{R}^{|\Phi_j| \times |\Phi_j|}$, is a symmetric matrix with each of the diagonal elements as the square of (9), and mutual elements as the products of composite tap ratios, e.g. $\hat{r}_{i'}^{ab} = r_{i'}^a r_{i'}^b$. In addition to (9), we define $\xi_{i',e}^{\phi} = u_{i',e}^{\phi} r_{i'}^{\phi}$ to linearize each of the diagonal elements using the big-M method as follows

$$\forall \phi \in \Phi, i' \in \mathcal{B}^s :$$

$$\hat{r}_{i'}^{\phi\phi} = (r^{\min} \times r_{i'}^{\phi}) + \Delta^r \sum_{e=0}^{\mathcal{E}} 2^e \xi_{i',e}^{\phi} \quad (11a)$$

$$0 \le \xi_{i',e}^{\phi} - r_{i'}^{\phi} \le (1 - u_{i',e}^{\phi})M \quad (11b)$$

$$0 \le \xi_{i',e}^{\phi} \le u_{i',e}^{\phi} M \quad (11c)$$

M can be replaced with $r^{\max}$ to avoid ill-conditioning. The nondiagonal elements can be treated similarly, each with two sets of binary variables, but are simplified with tap ratio products leveraging the problem decomposition as clarified in Section III-A.

Remark 1: For exposition, the uniform tap operation can be resembled by reformulating (10) to have a single tap ratio represented by one set of binary variables.

The separation of the two circuits is disambiguated by conserving power flows through bus i'.

C. Reactive Power Capability of PV Inverter

Off-unity PV inverters can be governed to supply or absorb reactive power. Fundamentally, power-electronic inverters can function with a variable power factor (PF) which has a continuous reactive power capability during on- and off-peak (STATCOM mode) periods. It is assumed that the DSO has a direct dispatch control over PVs. For a PV at $i \in \mathcal{B}^g$, the operating region based on solar power and bounded by the inverter's capacity is shown in Fig. 2c. This is translated into the following set of an SDP constraint and inequality constraints:

$$G_i = \begin{bmatrix} s^{\max} & s_i^{g,\phi} \\ (s_i^{g,\phi})^C & s^{\max} \end{bmatrix}$$

$$G_i \succeq 0 \qquad \forall \phi \in \Phi, i \in \mathcal{B}^g \quad (12a)$$

$$0 \le \mathrm{Re}(s_i^{g,\phi}) \le p^{\mathrm{for}} \qquad \forall \phi \in \Phi, i \in \mathcal{B}^g \quad (12b)$$

where $(^C)$ denotes the conjugate. Note that an oversized inverter is assumed, ensuring Var injection/absorption during peak solar generation.

Remark 2: The inverter's capacity limit constraint in (12a) is in Schur complement form [25], which is a generalization of the SOCP constraint, $(s_i^{\max})^2 \ge |s_i^{g,\phi}|^2$.

Considering the PV model in (12) and the constant-power demand s^d, the net load at bus $i \in \mathcal{B}^g$ then becomes

$$s_i = s_i^d - s_i^g. \quad (13)$$

D. The Multi-time Scheduling Problem

The problem is formulated with two sets of variables defined as follows:

$$\mathcal{X} := \{x|x = v, \ell, S, s^g\}, \quad \mathcal{Y} := \{y|y = r, \hat{r}, \xi, u\}$$

1) Objectives:

Substation Energy and Loss Reduction: Minimizing the energy purchase from the substation comes in the interest of reducing energy consumption and prioritizing the solar utility (minimizing curtailment). Reducing the real line losses incites control variables (tap positions and PV Var) to increase the voltage.

$$f_t(x) = c_{\mathrm{pri}} \left(\mathrm{Tr}\left(\mathrm{Re}\left(S_{01,t}\right)\right) + \sum_{(j,k) \in \mathcal{L}} \mathrm{Tr}\left(\mathrm{Re}\left(z_{ij} \ell_{ij,t}\right)\right) \right) \quad (14)$$
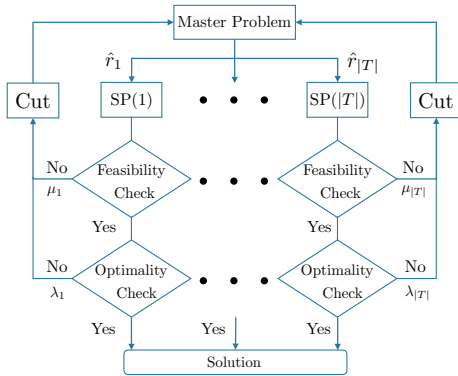
Fig. 3: GBD structure with temporally-decomposed subproblems

VRA Reduction: The change among intra-day ratio variables is minimized without imposing an initial state, so as to reduce the VR's mechanical switching, and thus maintenance costs.

$$h_t(y) = \sum_{i' \in \mathcal{B}^+} \sum_{\phi \in \Phi} c_{\mathrm{vr}} |\hat{r}_{i',t}^{\phi\phi} - \hat{r}_{i',t-1}^{\phi\phi}| \tag{15}$$

2) Overall Multi-Time Scheduling Problem:

$$\mathbf{VVO} := \min_{x,y} \quad \sum_{t=1}^{\mathcal{T}} f_t(x) + \sum_{t>1}^{\mathcal{T}} h_t(y) \tag{16a}$$

$$\text{s. t.} \quad v_{0,t} = V_{\mathrm{nom}} V_{\mathrm{nom}}^{\mathrm{H}} \tag{16b}$$

$$\underline{V}^2 \le \mathrm{diag}(v_{i,t}) \le \overline{V}^2 \quad \forall i \in \mathcal{B}^+ \tag{16c}$$

$$(2), (5), (6), (9)\text{-}(13), \quad x \in \mathcal{X}, \quad y \in \mathcal{Y} \tag{16d}$$

The ratio-voltage multiplication in (10) renders (16) nonconvex. In the next section, this nonconvexity is overcome by applying the GBD, which solves variables of $\mathcal{X}$ and $\mathcal{Y}$ in separate problems.

III. GENERALIZED BENDERS DECOMPOSITION

In this section, we apply the GBD [26], which was extended from [27], to decouple and solve the problem iteratively, thereby avoiding the aforementioned nonlinearity, and providing an effective approach to solve the MISDP problem. In each iteration, the solution to the master problem over $\mathcal{Y}$ is passed to the subproblems. In turn, the subproblems will be solved over $\mathcal{X}$ and optimality cuts will be created for the master problem. Conventionally, if the master renders one subproblem infeasible, the subproblem will be reformulated and a feasibility cut will be created.

Remark 3: Because of the wide range of tap ratios that VRs can take, the MP could pass a tap ratio to a single SP that results in the secondary-side voltage exceeding the upper bound or falling below the lower one, thus making the respective SP infeasible. In which case, a feasibility-check problem (FCP) should be formulated to create a feasibility cut whenever a single-time SP is infeasible, and ensure the MP avoids this particular combination of ratios. This prolongs the convergence, as the FCP is computed each time the MP oversteps or understeps a tap position at a certain phase and a certain time. Motivated by the work in [28], additional constraints are enforced on the tap ratios to respect the

secondary-side voltage limits relying on primary-side voltage parameters acquired from cumulated iterations.

A. Subproblem (SP)

The SP corresponding to the SDP-based BFM in the x-space only can succinctly be written as following.

$$\mathbf{SP} := \min_{x} \quad f_t^n(x) \tag{17a}$$

$$\text{s. t.} \quad v_{i',t}^n = \hat{r}_{i',t}^{*\,n} \odot v_{i,t}^n \tag{17b}$$

$$(2), (5), (6), (12), (13), (16b), (16c), \quad x \in \mathcal{X} \tag{17c}$$

where superscript $(*)$ distinguishes quantities obtained from the MP, and n denotes the iteration. The solutions to the SPs provide optimal Lagrangian multipliers $\lambda \in \mathbb{R}^{|\Phi_{i'}| \times |\mathcal{T}|}$ associated with the real diagonal of the secondary-side voltage.

Note for each VR, based on (11), there are 9 equality constraints. To streamline the cut-creating process, only three constraints related to the diagonal components are considered:

$$v_{i',t}^{\phi\phi^n} = \hat{r}_{i',t}^{\phi\phi,*\,n} \odot v_{i,t}^{\phi\phi^n} \quad : \text{dual variable } \lambda_{i',t}^{\phi^n} \tag{18}$$

The tap ratios in (9) are then utilized to realize the nondiagonal elements, and thereby the matrix $\hat{r}_{i'}$, to preserve voltage phase angles.

The upper bound of the original problem in (16) is composed of the aggregated solutions to the SPs and the fixed objective pertaining to the switching reduction.

$$\theta_{\mathrm{ub}}^n = \sum_{t=1}^{\mathcal{T}} f_t^n(x) + \sum_{t>1}^{\mathcal{T}} h_t^n(y^*) \tag{19}$$

B. Feasibility-Check Problem (FCP)

The FCP is formed by re-formulating the original problem such that a feasible solution is guaranteed for any given tap ratio. The objective function is to minimize the diagonal of the nonnegative auxiliary variable relaxing the ratio-voltage equality constraint, $g_t(w) = \mathrm{diag}(w_t)$.

$$\mathbf{FCP} := \min_{x,w} \quad g_t^n(w) \tag{20a}$$

$$\text{s. t.} \quad v_{i',t}^n = \hat{r}_{i',t}^{*\,n} \odot v_{i,t}^n + w_{i'}^n \tag{20b}$$

$$w_{i'}^n \succeq 0 \tag{20c}$$

$$(2), (5), (6), (12), (13), (16b), (16c), \quad x \in \mathcal{X} \tag{20d}$$

The dual variables, $\mu \in \mathbb{R}^{|\Phi_{i'}| \times |\mathcal{T}|}$, associated with the diagonal of the constraint (20b) are used to generate the feasibility cut.

C. Master Problem (MP)

With solutions to (17) and (20), the MP is formulated in y-space with constraints on the VRs.

$$\mathbf{MP} := \min_{y,\eta} \quad \sum_{t=1}^{\mathcal{T}} \eta_t^n + \sum_{t>1}^{\mathcal{T}} h_t^n(y) \tag{21a}$$

$$\text{s. t.} \quad \eta_t^n \ge f_t^N(x^*) + \sum_{i' \in \mathcal{B}^+} \sum_{\phi \in \Phi} v_{i,t}^{\phi\phi,*\,N} \lambda_{i',t}^{\phi^N} \left(\hat{r}_{i',t}^{\phi\phi^n} - \hat{r}_{i',t}^{\phi\phi,*\,N} \right)$$

$$N = 1, 2, \ldots, n-1, \quad t = 1, 2, \ldots, |\mathcal{T}| \tag{21b}$$

Algorithm GBD for Multi-time Scheduling

Step 1 $\rightarrow$ set $n = 1$ and $\theta_{\text{lb}}^1 = -\infty$, and pick any $y_t^1 \in \mathcal{Y}$

Step 2

 for $t = 1{:}T$ **do**

  solve SP

  if solution is feasible **then**

   update θ_{ub}^n and λ_t^n, and set $f_t^n(w) = \mu_t^n = 0$

  else

   solve FCP

   update μ_t^n, and set $f_t^n(x) = \lambda_t^n = 0$

  end if

 end for

Step 3 $\rightarrow$ check convergence:

 if $|\theta_{\text{ub}}^n - \theta_{\text{lb}}^n| \leq \epsilon$ **then**

  break

  disclose optimal results

 else

  continue

 end if

Step 4 $\rightarrow$ increase n by 1

  $\rightarrow$ solve MP, and update θ_{lb}^n and y_t^n

  $\rightarrow$ return to **Step 2**

$$0 \geq g_t^N(w^*) + \sum_{i' \in \mathcal{B}^+} \sum_{\phi \in \Phi} v_{i,t}^{\phi\phi,*^N} \mu_{i',t}^{\phi^N} \left(\hat{r}_{i',t}^{\phi\phi^n} - \hat{r}_{i',t}^{\phi\phi,*^N} \right)$$

$$N = 1, 2, \ldots, n-1, \qquad t = 1, 2, \ldots, |\mathcal{T}| \quad \text{(21c)}$$

$$\max(\mathbf{v}_{i,t}^{\phi\phi}) \hat{r}_{i',t}^{\phi\phi^n} \leq \overline{V}^2 \quad t = 1, 2, \ldots, |\mathcal{T}| \quad \text{(21d)}$$

$$\min(\mathbf{v}_{i,t}^{\phi\phi}) \hat{r}_{i',t}^{\phi\phi^n} \geq \underline{V}^2 \quad t = 1, 2, \ldots, |\mathcal{T}| \quad \text{(21e)}$$

$$(9), (11), \quad y \in \mathcal{Y} \quad \text{(21f)}$$

Constraints (21b)-(21c) are respectively the optimality and feasibility cuts. The multi-cut GBD yields the same result as the uni-cut GBD (a single cut over the entire scheduling horizon), but with faster convergence [29]. $\mathbf{v}_{i,t}^{\phi\phi} \in \mathbb{R}^{|N|}$ in (21d)-(21e) denotes a vector of primary-side voltage quantities obtained from accumulated iterations, $[v_{i,t}^{\phi\phi,*^1}, \ldots, v_{i,t}^{\phi\phi,*^{n-1}}]^{\text{T}}$, where max/min yields one quantity. Though not strictly removing infeasible tap selection, these two constraints reduce the search space and substantially improve the convergence process, and so removing them returns the classic GBD problem. The optimal solution to (21), θ_{lb}^n, is the lower bound of the original problem.

IV. NUMERICAL CASE STUDIES

In this section, the efficacy of the proposed scheduling problem is evaluated using multiple case studies on the radial structures of modified 37-bus and 123-bus feeders. The hourly normalized profiles shown in Fig. 4 are uniformly applied to real and reactive power demand and PV real power. Per-phase VRs are assumed to operate with 33 levels and a turns ratio varying from 0.9 to 1.1. The primary cost is assumed to be ($c_{\text{pri}} = 100\$/\text{MWh}$). Due to the uncertainty of the VR's life expectancy [30], their tap adjustment cost, c_{vr}, is unified for all VRs and varied to yield a targeted adjustment reduction, i.e. close to 50% reduction. Peak PV real power
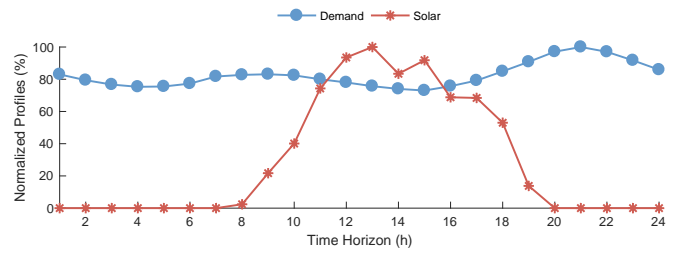

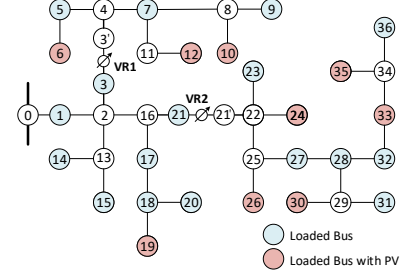Fig. 4: Hourly demand and solar profiles.

Fig. 5: Modified IEEE 37-bus feeder.

TABLE I: RESULTS FOR CASE I

Scenario	Sub. (MWh)	Loss (MWh)	Average Volt. (pu)	VRA Count
Baseline	49.8493	1.1982	1.0220	20
Unity-PF PVs	35.3499	0.9051	1.0246	60
0.9-PF PVs	35.1483	0.6929	1.0253	58

will capacitate oversized inverters to generate/absorb 46% of $|s^{\max}|$ as a reactive power.

A. Modified 37-bus Feeder

Fig. 5 depicts the modified IEEE 37-bus feeder with peak demand 2.7348 MVA and 0.9 PF. All lines are three-phase configured. Two VRs are placed as in Fig. 5 to compensate for voltages at remote buses. Nine three-phase PV are considered. Each PV inverter has a capacity of 250 kVA, and their combined penetration is 74% of the MW load.

Case I: Considering Primary Objective: The algorithm is computed with different scenarios to show the capability of VRs and PVs to attain minimum substation intake and line losses, and demonstrate the need for an extended objective. The switching penalty is set to zero ($c_{\text{vr}} = 0$). From Fig. 6a-6c and Table I, it can be seen that the baseline case with no PVs has the highest energy import and losses, but least tap switching. When unity-PF PVs are added, the VRs together with PV generation contribute to 29.1% and 24.5% of substation energy and loss reductions, albeit at the expense of excessive VRAs. PVs with off-unity PF, though contribute to a larger loss reduction during off-peak hours, do not seem to coordinate well with VRs or reduce the tap switching despite their reactive power capability. This signifies extending the objective to limit the VRAs.

The temporal variations of the average and range of the three-phase voltages are shown in Fig. 6d. Also, voltage magnitudes at phase C, whose MVA load accounts for 44.35% of the total load, are plotted in Fig. 6e-6f. It is noted that while
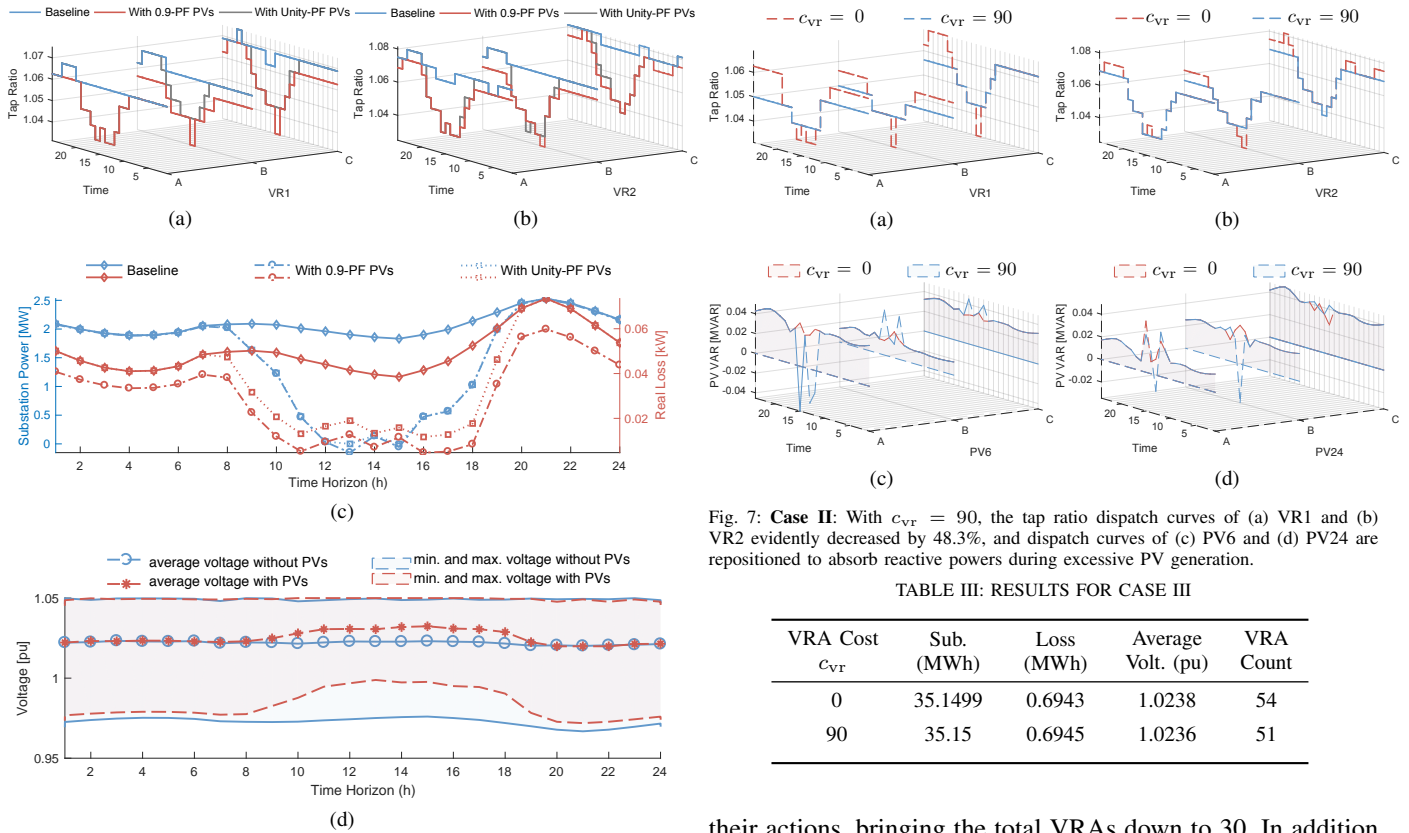
This article has been accepted for publication in a future issue of this journal, but has not been fully edited. Content may change prior to final publication. Citation information: DOI 10.1109/TSTE.2020.3007045, IEEE Transactions on Sustainable Energy

7

(a)
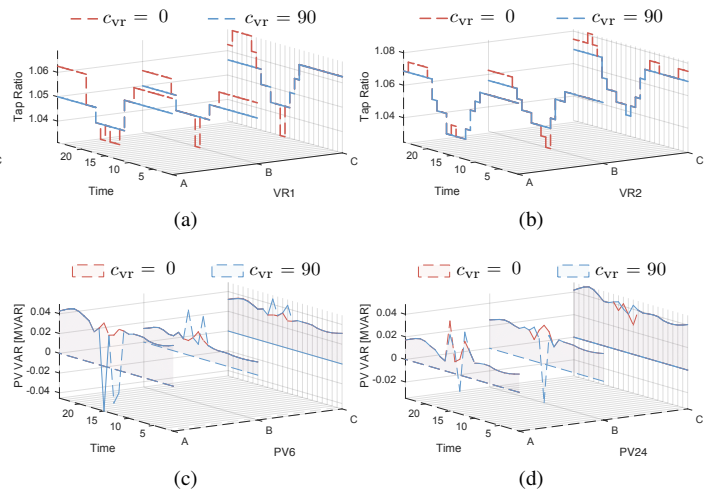

(b)

(c)

(a)

(b)

(c)

(d)

Fig. 7: **Case II**: With $c_{\mathrm{vr}} = 90$, the tap ratio dispatch curves of (a) VR1 and (b) VR2 evidently decreased by 48.3%, and dispatch curves of (c) PV6 and (d) PV24 are repositioned to absorb excessive reactive powers during excessive PV generation.

TABLE III: RESULTS FOR CASE III

VRA Cost c_{vr}	Sub. (MWh)	Loss (MWh)	Average Volt. (pu)	VRA Count
0	35.1499	0.6943	1.0238	54
90	35.15	0.6945	1.0236	51

(d)

Fig. 6: **Case I**: The tap ratio dispatch curves of (a) VR1 and (b) VR2 show that major VR switching occur during peak hours of PV generation. (c) Profiles of substation MW import/export, and line losses. 0.9-PF PVs further reduce the losses during off-peak hours. (d) Maximum, minimum and average voltage variations throughout the day. Nodal voltage variations of phase C (highest-loaded phase) voltages (e) without and (f) with PVs.

TABLE II: RESULTS FOR CASE II

VRA Cost c_{vr}	Sub. (MWh)	Loss (MWh)	Average Volt. (pu)	VRA Count	VRA Reduction
60	35.1518	0.7073	1.0254	37	36.2%
70	35.1521	0.7077	1.0247	34	41.4%
80 and 90	35.1513	0.7068	1.0238	30	48.3%

voltages are regulated within the $\pm 5\%$ limit, the VRs tap high increasing the secondary-side voltage near the upper bound.

Case II: Considering Extended Objective: In light of the results in Case I, we solve the scheduling problem with the extended objective to explore the possibility of urging PVs to collectively produce/absorb enough reactive power so as to reduce VR mechanical switching. Table II lists the results with three incremental switching costs, all of which are less than the primary objective cost ($c_{\mathrm{vr}} < c_{\mathrm{pri}}$). With $c_{\mathrm{vr}} = 90$, Fig. 7a-7b shows that VR1 spares 62.5% and VR2 spares 38.24% of

their actions, bringing the total VRAs down to 30. In addition to the longevity advantage, the percentage VRA reduction is proportional to the maintenance interval schedules [2], [31].

Being close to the VRs, the dispatch curves of PV6 and PV24 are also plotted in Fig. 7c-7d. It is evident that major alterations of reactive power dispatch occur at times when a steep tap action is spared. Also, VR taps are kept at lower positions during peak-loading hours with almost insignificant PV reactive power changes. In general, the VRA penalization heightened the PV reactive energy absorption by 105% compared to the unpenalized case, whereas the total reactive energy supply only decreased by 18.3%.

Case III: Comparison with Uniform Tap Operation: The results of nonuniform tap dispatch presented in Cases I and II are compared with the uniform tap operation, where phase tap positions of each VR switch uniformly. For this, the tap ratio is re-formulated to have one set of binary variables. Without the VRA penalization, the VRs with 0.9-PF PVs are scheduled with 54 VRAs in total, only 6% lower than the results in Case I. Enforcing the penalization with $c_{\mathrm{vr}} = 90$ reduces VRAs to 51, which is 70% more than the results in Case II. This shows that the nonuniform ratio modeling is more economic and amenable to the VRA reduction, even with lower values of c_{vr} as demonstrated in Case II.

B. Modified 123-bus Feeder

The proposed algorithm is also solved for the IEEE 123-bus feeder, which has multiple line configurations and a peak demand of 3.9833 MVA and 0.88 PF. The modified system shown in Fig. 8 involves five VRs and three PV plants. We introduce VR5 to test the scalability to a higher

This article has been accepted for publication in a future issue of this journal, but has not been fully edited. Content may change prior to final publication. Citation information: DOI 10.1109/TSTE.2020.3007045, IEEE Transactions on Sustainable Energy
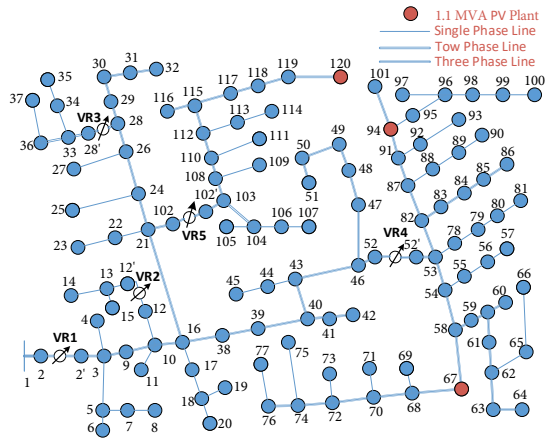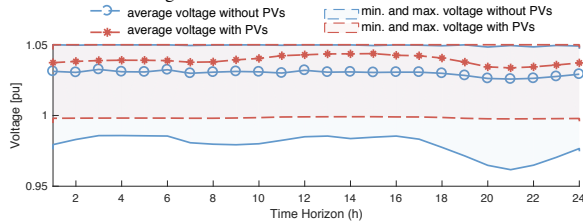
8

Fig. 8: Modified IEEE 123-bus feeder.

Fig. 9: 123-bus feeder maximum, minimum and average voltage levels of the baseline case and the 0.9-PF PV case with the penalized VRA.

TABLE IV: RESULTS FOR MODIFIED 123-BUS FEEDER

Scenario	Sub. (MWh)	Loss (MWh)	Average Volt. (pu)	c_{vr}	VRA Count	VRA Reduction
Baseline	71.4343	2.3637	1.0299	0	85	-
0.9-PF PVs	49.6419	1.2954	1.0399	0	64	24.7%
	49.6419	1.2954	1.0392	60	30	64.7%

number of VRs, and to regulate voltages of its downstream lateral. VR2 and VR3 are installed on single- and two-phase lines, respectively. The capacitor banks are assumed inactive. The capacity of each PV plant is 1.1 MVA, and their total penetration compounds to 86% of the MW load.

Table IV lists the results with and without 0.9-PF PVs along with the penalized-adjustment case. For this feeder, the baseline has the highest number of tap switching in which all VRs are engaged in the regulation. With PVs and unpenalized switching, the total VR adjustments reduced by 24.7%. The tap ratios of VR1 remained unaltered at 1.05. VR4 and VR5 constitute 70.3% of the total adjustments since the MVA loads, downstream their secondary sides, are 63% of the system's total load in addition to all PVs. When a VRA cost of 60 was invoked, VR2 and VR3 did not switch. Moreover, the total adjustments of VR4 and VR5 reduced by 64.7% from the baseline (53.12% from the unpenalized VRA case), and without inciting added energy import or losses. The temporal voltage variations (average and range) for the baseline and penalized switching cases are plotted in Fig. 9.

The VRAs of a single VR depend on the system topology, VR location, and the net demand change downstream from the VR. These factors not only differ from one feeder to another, but also from one VR to another [32]. From the previous case studies, we can deduce that larger values of c_{vr} are required for

TABLE V: NUMBER OF VARIABLES

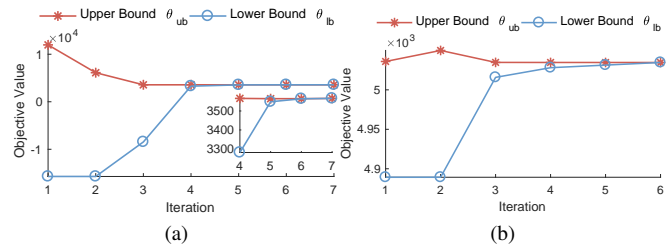| Modified 37-bus Feeder		Modified 123-bus Feeder	
SPs	MP	SPs	MP
25320	4824	45840	12450

(a)   (b)

Fig. 10: GBD convergence of (a) the 37-bus feeder case with $c_{\mathrm{vr}} = 90$, and (b) the 123-bus feeder case with $c_{\mathrm{vr}} = 60$.

the 37-bus feeder, where VRs are not cascaded, to spare 50% of VRAs. For the 123-bus feeder, where VR2-5 are cascaded by VR1, a smaller unified value of c_{vr} is sufficient to obtain a considerable VRA reduction.

C. Performance of the GBD-based Multi-time Scheduling

1) Computation: The problems are implemented in MATLAB 2016b with CVX [33], [34], where the SDP-based SPs are solved by Mosek solver [35], and the MILP-based MP is solved by Gurobi solver [36]. All simulations are performed on a laptop with Intel Core i7 at 2.7 GHz, 16 GB memory, and MAC OS 10.14. Table V lists the size of each problem for both feeders.

Table VI lists the average number of iterations, the average convergence values, and solving time costs averaged over all cases on each feeder for both single- and multi-time scheduling. The tolerance, ϵ, is chosen to be 1e−3. However, the problems converged to even lower error values shown in column 3. Though solved sequentially, parallel optimization computing of SPs is also possible [37].

2) SDP Exactness: For the rank-relaxed SDP problem, the exactness is customarily checked upon solving the problem by computing the eigenvalue ratio of each PSD matrix. If the ratio is small, it indicates that the PSD matrix has one dominant eigenvalue, which suffices to conclude that the solution is exact. The ratio is computed as in (22), where $|\mathrm{eig}_1| > |\mathrm{eig}_2|$, for all PSD matrices over the scheduling horizon. The last column of Table VI lists the ratio averaged over all cases.

$$\text{Ratios} = \sum_{t \in T} \sum_{\mathrm{eig} \in F_{i,j}^t} |\mathrm{eig}_2 / \mathrm{eig}_1| \tag{22}$$

The small ratio indicates that the relaxation is tight. Hence, the recovered optimal solutions are deemed AC feasible.

3) Comparison with Branch-and-Bound Method: To compare the proposed method with available solvers such as branch-and-bound method, we use Yalmip's built-in BNB solver [38] along with Mosek to solve the MISDP problem. First, the element-wise nonlinear constraints in (10) are linearized using additional sets of big-M inequality constraints in the flavor of (11). We attempt to solve the problem for a single-time dispatch, and a multi-time dispatch with reduced

TABLE VI: PERFORMANCE OF THE PROPOSED ALGORITHM

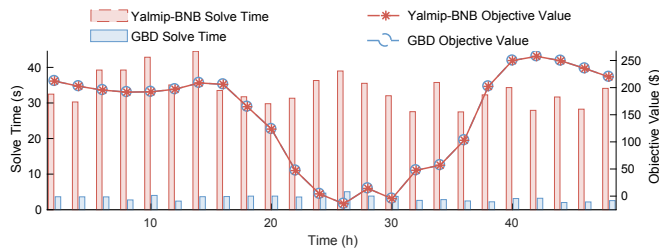| Scheduling	Average Iterations	Ave. Conv. $|\theta_{ub} - \theta_{lb}|$	Ave. Time (s)	Ave. Ratio
Modified IEEE 37-bus Feeder				
Single-time	4.95	6.91e-09	4.46	6.28e-09
Multi-time	9	1.04e-07	187.78	6.87e-09
Modified IEEE 123-bus Feeder				
Single-time	10.27	6.24e-09	10.41	7.48e-08
Multi-time	10	2.59e-08	266.54	1.45e-07

Fig. 11: Comparing the solve time and objective values of Yalmip-BNB and GBD method solutions for the modified 37-bus feeder. Evidently, the proposed problem outperforms that of the Yalmip-BNB.

VRAs on the modified 37-bus feeder. For the nonuniform tap control, where three sets of binary variables are required, the problem did not converge for both time operations. On the other hand, using the uniform tap control with one set of binary variables, the problem converges only for the single-time operation as in [20], [21] with average solve time of 33.85 s. The solve times and objective values are compared with the proposed GBD method in Fig. 11. It should be noted that the convergence is sensitive to the choice of big-M values. Randomly large or small values could also cause the problem to be non-convergent. In our experiments, we found that setting $M = 1000$ provides the fastest convergence. For the smallest consideration of multi-time operation (two time steps), the Yalmip-BNB problem is incapable of convergence even with maximizing BNB iterations to 50000. This also corroborates the capability of the proposed method to solve for multi-time operation with nonuniformly-operated taps.

V. CONCLUSION

This paper proposes a multi-time scheduling framework based on the SDP-based branch flow model to optimally dispatch discrete-based voltage regulators with nonuniform phase operation and off-unity inverters of photovoltaics, while considering the VRA costs. We circumvent the numerical complexities intrinsic to the MISDP problem and the nonlinear voltage-ratio relationship by the application of GBD with decoupled subproblems and a multi-cut master problem. We also propound additional constraints to accelerate the GBD convergence by narrowing the tap ratios with respect to secondary-side voltage limits. The case studies on the modified IEEE 37-bus and 123-bus test feeders evince the effectiveness of the proposed algorithm with a coordinated operation of VRs and PVs.

REFERENCES

[1] A. Nouri, A. Soroudi, and A. Keane, "Strategic scheduling of discrete control devices in active distribution systems," *IEEE Transactions on Power Delivery*, to be published.

[2] Y. P. Agalgaonkar, B. C. Pal, and R. A. Jabr, "Distribution voltage control considering the impact of pv generation on tap changers and autonomous regulators," *IEEE Transactions on Power Systems*, vol. 29, no. 1, pp. 182–192, 2014.

[3] M. E. Baran and M.-Y. Hsu, "Volt/var control at distribution substations," *IEEE Transactions on Power Systems*, vol. 14, no. 1, pp. 312–318, 1999.

[4] M. Chamana and B. H. Chowdhury, "Optimal voltage regulation of distribution networks with cascaded voltage regulators in the presence of high pv penetration," *IEEE Transactions on Sustainable Energy*, vol. 9, no. 3, pp. 1427–1436, 2018.

[5] E. Pourjafari and M. Reformat, "A support vector regression based model predictive control for volt-var optimization of distribution systems," *IEEE Access*, vol. 7, pp. 93 352–93 363, 2019.

[6] S. Paudyal, C. A. Cañizares, and K. Bhattacharya, "Optimal operation of distribution feeders in smart grids," *IEEE Transactions on Industrial Electronics*, vol. 58, no. 10, pp. 4495–4503, 2011.

[7] Q. Nguyen, H. V. Padullaparti, K.-W. Lao, S. Santoso, X. Ke, and N. Samaan, "Exact optimal power dispatch in unbalanced distribution systems with high pv penetration," *IEEE Transactions on Power Systems*, vol. 34, no. 1, pp. 718–728, 2019.

[8] W. Wu, Z. Tian, and B. Zhang, "An exact linearization method for oltc of transformer in branch flow model," *IEEE Transactions on Power Systems*, vol. 32, no. 3, pp. 2475–2476, 2017.

[9] F. U. Nazir, B. C. Pal, and R. A. Jabr, "A two-stage chance constrained volt/var control scheme for active distribution networks with nodal power uncertainties," *IEEE Transactions on Power Systems*, vol. 34, no. 1, pp. 314–325, 2018.

[10] S. R. Shukla, S. Paudyal, and M. R. Almassalkhi, "Efficient distribution system optimal power flow with discrete control of load tap changers," *IEEE Transactions on Power Systems*, vol. 34, no. 4, pp. 2970–2979, 2019.

[11] I. Alsaleh, L. Fan, and H. G. Aghamolki, "Volt/var optimization with minimum equipment operation under high pv penetration," in *2018 North American Power Symposium (NAPS)*. IEEE, 2018, pp. 1–6.

[12] R. Zafar, J. Ravishankar, J. E. Fletcher, and H. R. Pota, "Multi-timescale model predictive control of battery energy storage system using conic relaxation in smart distribution grids," *IEEE Transactions on Power Systems*, vol. 33, no. 6, pp. 7152–7161, 2018.

[13] P. Li, H. Ji, C. Wang, J. Zhao, G. Song, F. Ding, and J. Wu, "Coordinated control method of voltage and reactive power for active distribution networks based on soft open point," *IEEE Transactions on Sustainable Energy*, vol. 8, no. 4, pp. 1430–1442, 2017.

[14] M. Farivar and S. H. Low, "Branch flow model: Relaxations and convexification-part i," *IEEE Transactions on Power Systems*, vol. 28, no. 3, pp. 2554–2564, 2013.

[15] R. R. Jha, A. Dubey, C.-C. Liu, and K. P. Schneider, "Bi-level volt-var optimization to coordinate smart inverters with voltage control devices," *IEEE Transactions on Power Systems*, 2019.

[16] L. Gan and S. H. Low, "Convex relaxations and linear approximation for optimal power flow in multiphase radial networks," in *2014 Power Systems Computation Conference*. IEEE, 2014, pp. 1–9.

[17] E. Dall'Anese, H. Zhu, and G. B. Giannakis, "Distributed optimal power flow for smart microgrids," *IEEE Transactions on Smart Grid*, vol. 4, no. 3, pp. 1464–1475, 2013.

[18] B. A. Robbins, H. Zhu, and A. D. Domínguez-García, "Optimal tap setting of voltage regulation transformers in unbalanced distribution systems," *IEEE Transactions on Power Systems*, vol. 31, no. 1, pp. 256–267, 2016.

[19] M. Bazrafshan, N. Gatsis, and H. Zhu, "Optimal power flow with step-voltage regulators in multi-phase distribution networks," *IEEE Transactions on Power Systems*, 2019.

[20] Y. Liu, J. Li, L. Wu, and T. Ortmeyer, "Chordal relaxation based acopf for unbalanced distribution systems with ders and voltage regulation devices," *IEEE Transactions on Power Systems*, vol. 33, no. 1, pp. 970–984, 2018.

[21] Y. Liu, J. Li, and L. Wu, "Coordinated optimal network reconfiguration and voltage regulator/der control for unbalanced distribution systems," *IEEE Transactions on Smart Grid*, vol. 10, no. 3, pp. 2912–2922, 2018.

[22] I. Alsaleh, L. Fan, and M. Ma, "Mixed-integer sdp relaxation-based volt/var optimization for unbalanced distribution systems," in *2019 IEEE Power and Energy Society General Meeting (PESGM)*. IEEE, 2019, pp. 1–5.

[23] N. Daratha, B. Das, and J. Sharma, "Coordination between oltc and svc for voltage regulation in unbalanced distribution system distributed generation," *IEEE Transactions on Power Systems*, vol. 29, no. 1, pp. 289–299, Jan 2014.

[24] W. H. Kersting, *Distribution system modeling and analysis*. CRC press, 2012.

[25] J. A. Taylor, *Convex optimization of power systems*. Cambridge University Press, 2015.

[26] A. M. Geoffrion, "Generalized benders decomposition," *Journal of optimization theory and applications*, vol. 10, no. 4, pp. 237–260, 1972.

[27] J. F. Benders, "Partitioning procedures for solving mixed-variables programming problems," *Numerische mathematik*, vol. 4, no. 1, pp. 238–252, 1962.

[28] A. Nasri, S. J. Kazempour, A. J. Conejo, and M. Ghandhari, "Network-constrained ac unit commitment under uncertainty: A benders decomposition approach," *IEEE transactions on power systems*, vol. 31, no. 1, pp. 412–422, 2015.

[29] A. Schwele, J. Kazempour, and P. Pinson, "Do unit commitment constraints affect generation expansion planning? a scalable stochastic model," *Energy Systems*, pp. 1–36, 2019.

[30] H. Chen, H. Ngan, and Y. Zhang, *Power System Optimization: Large-scale Complex Systems Approaches*. John Wiley & Sons, 2016.

[31] S. Ghosh, F. Ding, J. Simpson, T. Harris, M. Baggu, H. G. Aghamolki, and W. Ren, "Techno-economic analysis for grid edge intelligence: A preliminary study on smart voltage regulator controls," in *2019 IEEE Power & Energy Society Innovative Smart Grid Technologies Conference (ISGT)*. IEEE, 2019, pp. 1–5.

[32] C. Li, V. R. Disfani, Z. K. Pecenak, S. Mohajeryami, and J. Kleissl, "Optimal oltc voltage control scheme to enable high solar penetrations," *Electric Power Systems Research*, vol. 160, pp. 318–326, 2018.

[33] M. Grant and S. Boyd, "CVX: Matlab software for disciplined convex programming, version 2.1," http://cvxr.com/cvx, Mar. 2014.

[34] M. Grant and S. Boyd, "Graph implementations for nonsmooth convex programs," in *Recent Advances in Learning and Control*, ser. Lecture Notes in Control and Information Sciences, V. Blondel, S. Boyd, and H. Kimura, Eds. Springer-Verlag Limited, 2008, pp. 95–110, http://stanford.edu/~boyd/graph_dcp.html.

[35] M. ApS, "The mosek optimization toolbox for matlab manual." 2017. [Online]. Available: https://docs.mosek.com/8.0/toolbox/index.html

[36] L. Gurobi Optimization, "Gurobi optimizer reference manual," 2020. [Online]. Available: http://www.gurobi.com

[37] X. Chen, E. Dall'Anese, C. Zhao, and N. Li, "Aggregate power flexibility in unbalanced distribution systems," *IEEE Transactions on Smart Grid*, vol. 11, no. 1, pp. 258–269, 2019.

[38] J. Löfberg, "Yalmip : A toolbox for modeling and optimization in matlab," in *In Proceedings of the CACSD Conference*, Taipei, Taiwan, 2004.

Lingling Fan (SM'08) received the B.S. and M.S. degrees in electrical engineering from Southeast University, Nanjing, China, in 1994 and 1997, respectively, and the Ph.D. degree in electrical engineering from West Virginia University, Morgantown, in 2001.

Currently, she is an Associate Professor with the University of South Florida, Tampa, where she has been since 2009. She was a Senior Engineer in the Transmission Asset Management Department, Midwest ISO, St. Paul, MN, form 2001 to 2007, and an Assistant Professor with North Dakota State University, Fargo, from 2007 to 2009. Her research interests include power systems and power electronics. Dr. Fan serves as the editor-in-chief for IEEE Electrification Magazine and an editor for IEEE transactions on Energy Conversion.

Ibrahim Alsaleh (S'16) received the B.S. degree in electrical engineering from the University of Hail, Hail, Saudi Arabia, in 2012, the M.S. and Ph.D. degrees in electrical engineering from the University of South Florida, Tampa, FL in 2016 and 2020. He is currently with the Department of Electrical Engineering, University of Hail. His current research interests include power system optimization and renewable energy integration.